Research Article

Dynamic response characteristics of the 67-type railway pontoon bridge

Cunbao Zhao[1] · Zhongming Jiang[2] · Bernt J. Leira[3] · Xuzhao Shi[1] · Zhaofeng Zheng[1]

Received: 11 December 2021 / Accepted: 23 September 2022
Published online: 20 October 2022

Abstract
In China at present, the 67-type railway pontoon bridge is part of the main reserve standard equipment that can be utilized for traffic emergency of cross-river bridges. Based on the potential flow theory and boundary element method (the three-dimensional source distribution method), this paper studies the dynamic response characteristics of the 67- type railway pontoon bridge under the action of waves and train loads (the live load of the Chinese Standard-18). First of all, the hydrodynamic characteristics based on application of other computation models applied in relation to floating bridges are compared with the results obtained by the present approach. Secondly, the effects of varying the related wave parameters (i.e. wave period and angle of incidence) on the dynamic response of the 67-type emergency railway pontoon bridge (as installed across the Ji Canal within the Beijing-Shanhaiguan line) are investigated. Finally, the load effects in the girder when this bridge is subjected to the action of various wave and train loads are analyzed. The calculation results indicate that the method proposed in this paper has good generality which enables it to perform a better analysis of the hydrodynamic characteristics of this kind of practical emergency pontoon.

Article highlights

1. Research on dynamic response for the major railway emergency pontoon in China are carried out;
2. The three-dimensional source distribution method and FEM is adopted;
3. Simulate traffic loads with the live load of the Chinese Standard-18.

Keywords 67-type railway pontoon bridge · Wave and train loads · hydrodynamic analysis · 3-D source distribution method · FEM

1 Introduction

As a country with frequent natural disasters, China is often affected by extreme environmental events such as typhoons, floods, mudslides, and so on, all of which pose serious threats to people's lives and their property. Especially during recent years, the frequent occurrence of earthquakes leads to bridge damage and to disruption of traffic. This implies that the associated water barriers cut the traffic link between the epicenter and the outside world. As a consequence, the

✉ Cunbao Zhao, zhaocb@stdu.edu.cn | [1]State Key Laboratory of Mechanical Behavior and System Safety of Traffic Engineering Structures, Shijiazhuang Tiedao University, Shijiazhuang 050043, China. [2]China Railway Fifth Survey and Design, Institute Group Co. Ltd.,, Beijing 102600, China. [3]Department of Marine Technology, Norwegian University of Science and Technology, NO-7491 Trondheim, Norway.

rescue work after the earthquake becomes increasingly difficult, and many victims in the disaster area will die because they can not get active and effective assistance in time. It is realized that rapid recovery of the bridge crossings and opening of the access roads are generally of key importance in order to minimize disaster losses. However, it is not realistic to repair a destroyed bridge in a short time due to the complexity associated with deep, large spans as well as difficult subsea terrain conditions. Therefore, it is urgent that emergency bridge structures are available that can be quickly installed in order to accomplish a rapid restoration of the traffic. The 67-type railway pontoon bridge is found to be an efficient solution to these challenges [1].

The hydrodynamic properties of floating bridges have been the subject of many studies in the literature [2]. Xin [3] proposed a mechanical calculation model for a railway floating bridge, which simplified the actual structure of the floating bridge as a composite frame system which consisted of a number of beams. This system comprised different cases of rigid frames, truss and rigid joints, hinged connections, semi-hinged connections and various forms of supports. Zhang et al. (2007) [4] used the beam theory and boundary element method to study the hydrodynamic characteristics of a ribbon pontoon bridge under moving loads for different water depths. The results show that the water depth has little effect on the hydroelastic natural frequencies and on the dynamic response of floating bridges that were studied. Mukherji (1995) [5] studied the hydroelastic dynamic response of a floating bridge with separate pontoons under the action of waves based on the theory of beams on elastic foundation. The dynamic response analysis was performed both in the time and the frequency domain. Shi et al. (2003) [6] and Wang (2013) [7] studied the structural vibration of floating bridges under the action of moving loads, based on neglecting the influence of the end guide structure on the bridge. The bridges were modeled as a simply supported beam resting on an elastic foundation. The dynamic response of a free-floating uniform beam under the action of a moving load has also been computed by application of finite element software. Dynamic response of floating bridges subjected to wave action has been analyzed by a number of researchers, see e.g. Hartz et. al. [8], Langen and Sigbjørnsson [9], Watanabe [10], Li et al. [11] and Giske et. al. (2017) [12]. However, it is not advisable to simply use the elastic foundation beam theory for analysis. This is due to fluid–structure interaction, including scattering and diffraction effects. This effect has also been addressed for other floating bridge concepts e.g. by Xiang et. al. [13]. Lin [14]computed the natural frequencies, mode shapes and dynamic response of floating bridges subjected to vehicle loads by implementing self-developed 'rigid-rigid' beam elements and 'rigid- articulated' beam elements within the finite element software ABAQUS. Wang et al. (2013) [15] analyzed the influence of moving loads with variable speed on the dynamic response of floating bridges based on the finite element method. Internal force response curves were obtained for both hinged and clamped floating bridges subjected to different loads and different variable vehicle speeds. Cheng et al. [17], Sha et al. [18] and Dai et al. [19] studied structural responses of a complex end-anchored curve bridge under action of wave load and wind load, consisting of a cable-stayed high bridge part and a low bridge part supported by 19 pontoons.

The 67-type railway boat bridge is the most mature transportation emergency railway pontoon bridge in China. As its main R&D personnel, Deji [21] introduced the project's R&D process in detail and several verification experiments of opening to traffic. Due to the fast and cost-effective erection of the 67-type emergency railway pontoon bridge, China's relevant departments have a large reserve of such bridge components (See Appendix I for a historic account of this bridge type). It has become the first choice in order to cross water barriers after disaster has struck. Historically, it has bought valuable time for rescue operations and hence avoided casualties as well as property losses. Although application of the 67-type emergency railway pontoon bridge is becoming more and more extensive, and although its role is becoming more and more prominent, its safety and feasibility are often verified by means of traffic tests. There is still a large gap in research regarding the dynamic characteristics of this type of pontoon bridge. In previous studies of other floating bridges, simplified models of the floating bridge based on the theory of beams on elastic foundation are frequently applied. This implies that only the buoyancy effect of the static fluid on the railway floating bridge is considered, i.e. the effect of water is approximated into a collection of spring supports, while the effects of waves on the floating bridge are ignored. In fact, structures floating on the water surface will be elastically deformed and sometimes even damaged due to the combined action of wind, waves, and currents. Therefore, dynamic response analysis of structures subjected to such loads becomes a more challenging task. The spans of the floating bridges are frequently extensive, and they are usually composed of several pontoons connected by rigid or flexible members. Furthermore, the elastic deformations caused by the waves are usually characterized by significant dynamic amplification. Accordingly, it is necessary to study the dynamic response of this type of floating bridge when it is subjected to wave action.

Safi. Mohamad et al. [16]. proposed to analyze the hydrodynamic characteristics of the floating bridge by using the three-dimensional singular point source method based on potential flow theory and with the aid of the boundary element method. The physical model of the

pontoon bridge built in this paper is completely based on the design drawings of the 67-type railway pontoon bridge, and it is the closest model to the actual pontoon bridge so far. The hydrodynamic characteristics of the 67-type emergency railway pontoon bridge were studied by using the Green's formula method and both frequency and time domain methods. The response to live loads representing the relevant train type (the standard live load of Chinese Standard-18) [20] was also considered. In the next section, we consider to establish the mathematical model for pontoon bridge in flow field and to solve the governing equations for flow field and the pontoons structures, Sect. 3 shows the verification results of numerical example for the Bergsøysund pontoon bridge in Norway and a case study of the dynamic characteristics of the 67-type railway bridge crossing at the Jiyun Canal of the Jingshan Line during the emergency installation following the Tangshan earthquake in 1976. In Sect. 4, we present the overall research results of this paper and some qualitative evaluations.

2 Mathematical model

2.1 Governing equations of flow field

The structure of the 67-type emergency railway pontoon bridge is a split bridge joint, which consist of the parts extending into the river, the transition, the movable trestle bridge and the fixed trestle bridge, as shown in Fig. 1. It is connected by a continuous beam system consisting of a steel truss beam. When the corresponding highway equipment is added for each part, it can be applied as a dual-purpose pontoon bridge for both road and railway vehicles [1–3]. See the literature for information on detailed parameters of the 67-type emergency railway pontoon bridge [2].

It is assumed that the entire pontoon bridge is supported by N pontoons resting on a water surface for which the distance to the bottom is constant, and each of these pontoons move in six degrees of freedom under the action of a harmonic wave (the incident water wave is along the direction toward the blunt head of the floating pier). The flow field has no rotation, the fluid is incompressible, and the total potential of the flow field is written as

$$\Phi(x,y,z,t) = \phi(x,y,z)e^{-i\omega t} \tag{1}$$

where $\phi(x,y,z)$ is the space part of the potential function, and ω is the circular frequency of the wave.

When there are N floating bodies in the flow field, the potential function usually includes the incident wave velocity potential, the diffraction wave velocity potential and the perturbation velocity potential generated by each floating body moving in six degrees of freedom. This gives a total of 2 + 6 N term, that is

$$\phi = -i\omega\left[(\phi_0 + \phi_7)\zeta_a + \sum_{m=1}^{N}\sum_{j=1}^{6}\left(X_j^m\phi_j^m\right)\right] \tag{2}$$

where ϕ_0 is the velocity potential of the incident wave, ϕ_7 is the velocity potential of the diffracted wave and ϕ_j^m is the velocity potential generated when the *mth* floating body unit moves in degree of freedom number j ($j = 1, 2, \ldots, 6$), ζ_a is the amplitude of the incident wave and the diffracted wave, and X_j^m is the amplitude corresponding to the corresponding unit velocity potential ϕ_j^m .

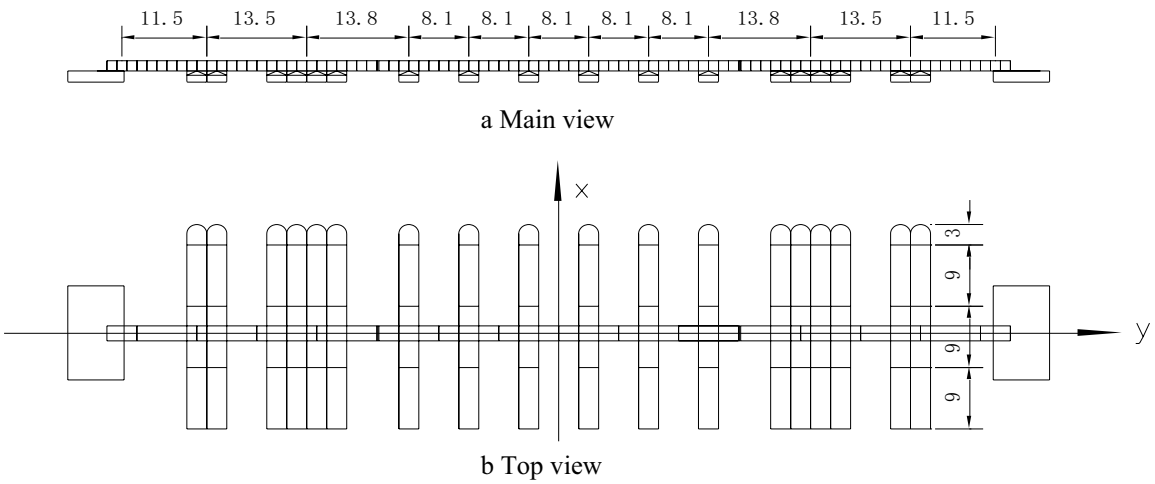

Fig. 1 Layout schematic of the 67-type railway bridge (Unit: m)

For a regular wave, the velocity potential of the incident wave can usually be described on the following form,

$$\phi_0 = \left(\frac{g}{\omega^2}\right)\frac{\cosh\left[k(z+h)\right]}{\cosh(kh)}e^{ik(x\cos\beta+y\sin\beta)} \tag{3}$$

where k is the wave number, h is the water depth, g is the acceleration of gravity, and β is the angle between the propagation direction of the incident wave and the positive direction of the X-axis.

The circular frequency ω of the wave and the wave number k satisfy the following dispersion equation

$$k\tanh(kh) = \omega^2/g \tag{4}$$

Furthermore, the velocity potential function should satisfy the Laplace equation

$$\nabla^2\phi = 0 \tag{5}$$

which represents incompressibility of the fluid.

2.2 Boundary conditions for the flow field

The velocity potential should also satisfy the following boundary conditions:

(1) Boundary conditions at the linearized free liquid surface

$$\frac{\partial\phi}{\partial z} = \left(\frac{\omega^2}{g}\right)\phi(z=0) \tag{6}$$

(2) Boundary conditions at the bottom of the river

$$\frac{\partial\phi}{\partial z} = 0(z=-h) \tag{7}$$

(3) Boundary conditions on the wet surface of the floating bodies.

Because of the existence of the floating body in the flow field, its surface S will also give rise to boundary conditions for the flow field. Assuming that the wet surface of the floating body meets the "*impermeability*" condition, the corresponding kinematic boundary conditions are

$$\left(\frac{\partial\phi}{\partial n}\right)_s = v_n \tag{8}$$

This condition expresses that the orthogonal component $(\partial\phi/\partial n)$ of the fluid velocity on the wet surface S of the floating body is equal to the orthogonal component v_n of the speed of the floating body.

Further, when the floating body is at rest, the boundary conditions on the wet surface are expressed as

$$\begin{aligned}
&\frac{\partial\phi_0}{\partial n} + \frac{\partial\phi_7}{\partial n} = 0\\
&\frac{\partial\phi_j^m}{\partial n} = n_j^m \ \ on\ \ the\ \ S^m\ \ plane\\
&\frac{\partial\phi_j^m}{\partial n} = 0\ \ on\ \ the\ \ S^i\ \ plane\ i \neq m
\end{aligned} \tag{9}$$

here, n_j^m represents the direction cosine of the *m'th* unit in the *j'th* motion mode, S^m and S^i are the *mth* and i*th* divided wet surface panel respectively. The range of values for m is from 1 to N, and

$$\begin{aligned}
&n_1^m = \cos(n^m, x^m)\ n_2^m = \cos(n^m, y^m)\ n_3^m = \cos(n^m, z^m)\\
&n_4^m = (y^m - y_G^m)n_3^m - (z^m - z_G^m)n_2^m\\
&n_5^m = (z^m - z_G^m)n_1^m - (x^m - x_G^m)n_3^m\\
&n_6^m = (x^m - x_G^m)n_2^m - (y^m - y_G^m)n_1^m
\end{aligned} \tag{10}$$

here, x_G^m, y_G^m and z_G^m represent coordinate values of the center of gravity for the submerged volume m in the rectangular coordinate system $O-XYZ$, and (x^m,y^m,z^m) represent coordinate values of the control point on the wet surface of m.

(4) Radiation boundary conditions at infinity

$$\lim_{r\to\infty}\left[\sqrt{r}\left(\frac{\partial\varphi}{\partial r} - ik\varphi\right)\right] = 0 \tag{11}$$

where r represents the horizontal distance from the source of disturbance.

2.3 The solution for the flow field velocity potentials

According to the boundary element method, the unknown potential functions can be expressed as

$$\varphi_j(x,y,z) = \frac{1}{4\pi}\iint_S \sigma_j(\xi,\eta,\zeta)G(x,y,z;\xi,\eta,\zeta)ds\ (j=1,2,\ldots,7) \tag{12}$$

In this formula, $\varphi_j(x,y,z)$ represents the unknown potential function at any point (x,y,z) in the flow field, $\sigma_j(\xi,\eta,\zeta)$ is the source intensity distributed on the wet surface S of the floating body, G is a Green's function that satisfies various boundary conditions and continuity equations.

For a three-dimensional flow field in finite water depth, the Green's function can be expressed as

$$G = 2\pi \frac{k^2 - \nu^2}{k^2 h - \nu^2 h + \nu} \cosh(k(z+h)) \cosh(k(\zeta+h)) \left(Y_0(kR) - \mathrm{i}J_0(kR)\right) + 4\sum_{i=1}^{\infty} \frac{\mu_i^2 + \nu^2}{\mu_i^2 h + \nu^2 h - \nu} \cos\left(\mu_i(z+h)\right) \cos\left(\mu_i(\zeta+h)\right) K_0(\mu_i R) \tag{13}$$

or

$$G = \frac{1}{-} \tag{14}$$

In these formulas, h is the water depth; k is the wave number; J_0, Y_0, K_0 respectively represent the zero-order values of the Bessel function of the first type, the Bessel function of the second type; the modified Bessel function of the second type; *P.V.* represents the principal value integral of the function; and

$$\begin{cases} r = \sqrt{(x-\xi)^2 + (y-\eta)^2 + (z-\zeta)^2} \\ r_1 = \sqrt{(x-\xi)^2 + (y-\eta)^2 + (z+2h+\zeta)^2} \\ R = \sqrt{(x-\xi)^2 + (y-\eta)^2} \end{cases} \tag{15}$$

$$\mu_i \tan\left(\mu_i h\right) + \nu = 0 \tag{16}$$

$$\nu = \frac{\omega^2}{g} = k \tanh(kh) \tag{17}$$

Although the expressions for the two Green's formulas are consistent, they still have different relationships to the specific calculation process, which mainly depends on the value of the variables R in Eq. (15). Comparing the two expressions, expression (13) is relatively simple to calculate, but when $R=0$, K_0 is close to infinity, and expression (14) should be used for the calculation instead. In another words, expression (14) is suitable for the case where the R value is very small or $R=0$.

According to Green's third formula, the normal gradient of the velocity potential function on the wet surface of the floating body can be expressed as

$$\frac{\partial}{\partial n}\varphi_j^m(P) = -\frac{1}{2}\sigma_j^m(P) + \frac{1}{4\pi}\sum_{n=1}^{N} \iint_{S^n} \sigma_j^m(Q) \frac{\partial}{\partial n} G(P,Q) ds \tag{18}$$

here, P, Q are the two relevant points in the flow field, and N is the total number of discrete elements on the wet surface.

Substituting this formula into the boundary condition (9) at the surface of the object and simplifying, the following is obtained,

$$-\frac{1}{2}\sigma_7(P) + \frac{1}{4\pi}\sum_{k=1}^{N} \iint_{S^n} \sigma_7(Q) \frac{\partial}{\partial n} G(P,Q) ds = -\frac{\partial \varphi_0}{\partial n}$$

$$-\frac{1}{2}\sigma_j^m(P) + \frac{1}{4\pi}\sum_{k=1}^{N} \iint_{S^n} \sigma_j^m(Q) \frac{\partial}{\partial n} G(P,Q) ds = \begin{cases} n_j^m & P \in m \\ 0 & P \notin m \end{cases} \tag{19}$$

By solving Eq. (18), the specific value of the intensity of the unknown sources can be determined. However, this method is based on discretizing the surface into triangular or quadrilateral panels, so it is only applicable to flat elements. In general, for elements of arbitrary shape i^*, the source intensity equation can be expressed as

$$-\frac{1}{2}(\sigma_j^m)_{i*} + \frac{1}{4\pi}\sum_{n=1}^{N}\sum_{i=1}^{E_n} \iint_{\Delta S_i^n} (\sigma_j^m)_i \frac{\partial}{\partial n} G(i*, i) ds = \begin{cases} (-\frac{\partial \varphi_0}{\partial n})_{i*} & j = 7 \\ (n_j^m)_{i*} \quad i* \in m, & j = 1,2,3\cdots 6 \\ 0 \quad i* \notin m, & j = 1,2,3\cdots 6 \end{cases} \tag{20}$$

In this formula, E_n is the number of panel elements for the *nth* object, and ΔS_i^n is the area of panel element number i for object number n, $(\sigma_j^m)_i$ represents the source intensity for panel number i for object number m corresponding motion mode number j, $\left(-\partial\varphi_0/\partial n\right)_{i^*}$ is the normal velocity of the incident wave for panel number i^*.

2.4 Governing equations for the pontoons and the bridge structure

Considering that the floating bridge is subjected to hydrodynamic excitation forces, additional inertia forces and damping forces, the equation of motion for the floating structure subjected to wave and other loads can be expressed as follows:

$$(\mathbf{M} + \mathbf{M_a})\ddot{\mathbf{X}} + \int_{-\infty}^{t} \mathbf{R}(\mathbf{t} - \boldsymbol{\tau})\dot{\mathbf{X}}\mathrm{d}\tau + \mathbf{K}\mathbf{X} = \mathbf{F}(\mathbf{t}) + \mathbf{F_n}(\mathbf{t}) \tag{21}$$

In this formula, $\mathbf{M}$ is a generalized mass matrix, $\mathbf{M_a}$ is an additional mass matrix independent of the circular frequency, $\mathbf{R}$ is the hysteretic damping matrix, $\mathbf{K}$ is the stiffness matrix, $\mathbf{X}$ is the time-varying motion of the body, t, τ are time, $\mathbf{F}(\mathbf{t})$ is the first-order wave excitation force, and $\mathbf{F_n}(\mathbf{t})$ designates the other external forces. Furthermore

$$R_{kj} = \frac{2}{\pi}\int_0^{+\infty} b_{kj}(t)\cos\omega t \mathrm{d}t \tag{22}$$

$$(M_a)_{kj} = a_{kj}(\omega^*) + \frac{1}{\omega^*}\int_0^{+\infty} R_{kj}(t)\sin(\omega^* t)\mathrm{d}t \tag{23}$$

where a_{kj} is called the additional quality factor, $a_{kj} = -\rho \mathrm{Re}\left[\iint_S \varphi_j n_k ds\right]$, b_{kj} is called the wave damping coefficient, $b_{kj} = -\rho\omega \mathrm{Im}\left[\iint_S \varphi_j n_k ds\right]$, and ω^* is the selected value of the circular frequency.

When the various potential functions have been determined, the hydrodynamic force in the k-direction acting on the floating body can be expressed by the following formula

$$F_k = -\rho\zeta_a\omega^2 e^{-i\omega t} \iint_S (\varphi_0 + \varphi_7) n_k ds (k = 1, 2, \ldots, 6) \tag{24}$$

Due to the bridge girder connecting two adjacent pontoons being a double truss structure, the connecting girder and the two adjacent pontoons can usually be treated as a "super-unit" when the floating bridge is analyzed as a complete structure. In this way, the stiffness matrix of the pontoon bridge can be derived by using 3-D beam element modeling. Based on 6 degrees of freedom at each of the end points, the stiffness matrix of any element within the bridge deck can be expressed as follows

$$\mathbf{K_b} = \begin{bmatrix} \mathbf{K_{b11}} & \mathbf{K_{b12}} \\ \mathbf{K_{b21}} & \mathbf{K_{b22}} \end{bmatrix} \tag{25}$$

Here, every $\mathbf{K_{b11}}$, $\mathbf{K_{b12}}$, $\mathbf{K_{b21}}$ and $\mathbf{K_{b22}}$ represents a 6×6 square matrix. The above stiffness matrix is applicable between the two ends of the element. However, the equation of motion (21) is referred to the center of gravity of the pontoon. Therefore, the stiffness matrix should be transformed into a coordinate system passing through the center of gravity (COG). The corresponding stiffness matrix referred to the COG coordinate system can then be written as

$$\mathbf{K_i} = \begin{bmatrix} \mathbf{T_m^T K_{b11} T_m} & -\mathbf{T_m^T K_{b12} T_n} \\ -\mathbf{T_n^T K_{b21} T_m} & \mathbf{T_n^T K_{b22} T_n} \end{bmatrix} \tag{26}$$

where

$$\mathbf{T_m} = \begin{bmatrix} 1 & 0 & 0 & 0 & z_m & -y_m \\ 0 & 1 & 0 & -z_m & 0 & x_m \\ 0 & 0 & 1 & y_m & -x_m & 0 \\ 0 & 0 & 0 & 1 & 0 & 0 \\ 0 & 0 & 0 & 0 & 1 & 0 \\ 0 & 0 & 0 & 0 & 0 & 1 \end{bmatrix} \tag{27}$$

In this matrix, x_m, y_m and z_m are the coordinates of the P_m point in the $G^m - x_b^m y_b^m z_b^m$ coordinate system (A coordinate system fixed to a single floating body mth, the form of $\mathbf{T_n}$ is the same).

The element stiffness matrices are assembled in the system stiffness matrix of the structure which can be finally written as follows,

$$\mathbf{K} = \begin{bmatrix} \ddots & & & \mathbf{0} \\ & \mathbf{K}_{i11} + \mathbf{K}_{(i-1)22} & \mathbf{K}_{i12} & \\ & \mathbf{K}_{i21} & \mathbf{K}_{22} + \mathbf{K}_{(i+1)11} & \\ \mathbf{0} & & & \ddots \end{bmatrix} \tag{28}$$

The notation is similar to formula (27), where K_{i11}, $K_{(i-1)22}$, K_{i12}, … are 6×6 square matrices.

The additional mass matrix contains both the mass of the pontoon and the bridge deck. For each pontoon, its inertia matrix is the same as for a general floating body. If the mass of the panel element is ideally concentrated at one point, the mass matrix of any bridge deck element can be written as

$$\mathbf{M_b} = \begin{bmatrix} \mathbf{M_{b11}} & \mathbf{0} \\ \mathbf{0} & \mathbf{M_{b22}} \end{bmatrix} \tag{29}$$

Here, $\mathbf{M_{b11}} = \mathbf{M_{b22}} = \mathbf{E_{6\times6}}\left(\frac{m_b}{2}\right)$, m_b is the total mass of the unit.

The elements in the generalized mass matrix are transformed into the coordinate system of the center of gravity of the pontoon and then added into the overall mass matrix of the structure.

$$\mathbf{M} = \begin{bmatrix} \ddots & & & \mathbf{0} \\ & \mathbf{M_{i11}} + \mathbf{M_{(i-1)22}} & \mathbf{M_{i12}} & \\ & \mathbf{M_{i21}} & \mathbf{M_{22}} + \mathbf{M_{(i+1)11}} & \\ \mathbf{0} & & & \ddots \end{bmatrix} \tag{30}$$

2.5 Moving loads

It is now assumed that the train is always in contact with the bridge girder when travelling across the bridge deck. Furthermore, the impact of the train's elasticity and damping characteristics on the pontoon and train motion is neglected, and then the inertial force caused by the gravity of the train and by its motion will generate a distributed force acting on the surface of the support structure.

For the gravitational load of a train, its force on each pontoon can be expressed as:

$$\left\{\mathbf{F^{ext}}\right\}_1 = \sum \delta\left(\mathrm{num}\left(E_{ve}\right) - \mathrm{num}\left(E_{vt}\right)\right) \iint_{S_{ve}} [\mathbf{N}]^{\mathbf{T}} \left\{\mathbf{p_t}\right\} \mathbf{dS_{ve}} \tag{31}$$

Here, δ represents the Dirac function, **num** represents the number of surface units that are subjected to the load of the train, Σ represents summation over the number of surface elements carrying the load of the train, E_{vt} represents all the surface elements that carry the load of the train at time t, E_{ve} is a unit in E_{vt}, and its area is S_{ve},

$\{p_t\} = P/A_t$ represents the density of the gravity distribution over the surface unit subjected to the trainload at time t, P and A_t represent separately the gravity of the train unit and the area of the structural surface subjected to the trainload at time t, $[\mathbf{N}]^T$ is a matrix of normal unit vectors for each surfel.

For the inertial force caused by train motion, the force it produces on the pontoons can be expressed as:

$$\{\mathbf{F}^{\mathbf{ext}}\}_2 = \sum -\delta(\mathrm{num}(E_{ve}) - \mathrm{num}(E_{vt})) \iint_{S_{ve}} [\mathbf{N}]^{\mathbf{T}} \rho_t [\mathbf{N}] \{\ddot{\mathbf{d}}\} \mathbf{dS_{ve}} \tag{32}$$

Here, $\rho_t = p_t/g$ represents the mass distribution density of the vehicle-mounted mass on the loaded unit. Assuming that the surface elements subjected to the train loads have a uniform thickness t_{ve}, Eq. (32) can be further expressed as:

$$\{\mathbf{F}^{\mathbf{ext}}\}_2 = -[\mathbf{M_v}]\{\ddot{\mathbf{D}}\} \tag{33}$$

In the formula:

$$[\mathbf{M_v}] = \sum \delta(\mathrm{num}(E_{ve}) - \mathrm{num}(E_{vt}))[\mathbf{m_{ve}}] \tag{34a}$$

$$[\mathbf{m_{ve}}] = \iiint_{V_{ve}} [\mathbf{N}]^{\mathbf{T}} \frac{\rho_t}{S_{ve} \cdot t_{ve}} [\mathbf{N}] \{\ddot{\mathbf{d}}\} \mathbf{dV_{ve}} \tag{34b}$$

where $V_{ve} = S_{ve} \cdot t_{ve}$ represents the volume of the train loading unit, $[\mathbf{M_v}]$ represents the moving mass matrix caused by the train inertia force. It only has non-zero elements for the degrees of freedom of the element subjected to the train loads at time t, and the remaining elements are all zero.

3 Numerical examples

3.1 The Bergsøysund bridge verification study

In the paper by Seif Mohammad et al. [16], the Bergsøysund pontoon bridge in Norway was appropriately simplified (e.g. the curved arch-bridge is simplified into a straight bridge), and the corresponding hydrodynamic analysis was carried out by application of relevant computer software. The variation of the heave excitation force (i.e. F3 in the vertical direction) acting on each floating pontoon as a function of the circular wave frequency ω was computed. The corresponding maximum vertical acceleration of each pontoon was also evaluated for waves with different angles of incidence relative to the bridge axis.

The total length of the floating bridge is 800 m, and there are 7 floating pontoons spaced at a distance of 100 m. The bridge girder is comprised of a tubular steel truss. It is assumed that all pontoon shapes and dimensions are the same, and the characteristics are given in Table 1. Approximate estimates of relevant parameters for the bridge deck section are found in Table 2, and the calculation model is shown in Fig. 2. The average water depth at this section is 320 m and the wave height is 0.6 m.

Figures 3, 4, 5 show the comparison of calculation results of the vertical excitation forces for the pontoon at the middle of the bridge (i.e. Pontoon No.4) when the incident angle (the horizontal angle between the direction of water wave propagation and the transverse axis of the pontoon) is 0°, 22.5°, and 45°. It can be seen that the calculation results for the two analysis results are in good agreement. Figure 6 shows the maximum vertical acceleration for each pontoon when the angle

Table 1 Main dimension of pontoons

Length/m	Width/m	Draft/m	Displacement/m^3
34.0	20.0	4.0	2 720.0
Transverse metacenter /m	Longitudinal metacenter /m	Transverse radius of gyration /m	Longitudinal radius of gyration /m
4.66	22.6	6.1	10.0

Table 2 The cross-sectional characteristic parameters of the bridge structure

I_y(moment of inertia of section y-axis)/m^4	I_z(moment of inertia of section z-axis)/m^4	A(area of section)/m^2
4.66	7.88	0.476

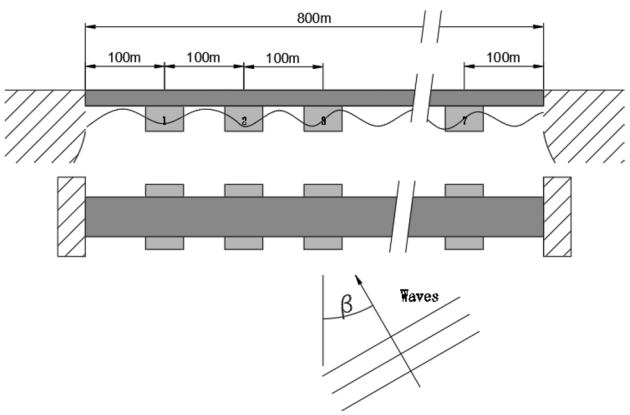

Fig. 2 The simplified calculation model of the Norwegian Bergsøysund bridge applied in Ref [16]

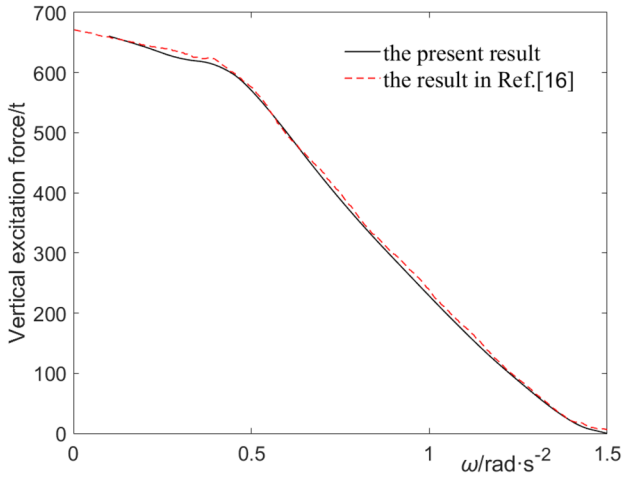

Fig. 3 Influence of wave frequency on the vertical force for the 4th pontoon (β=0°)

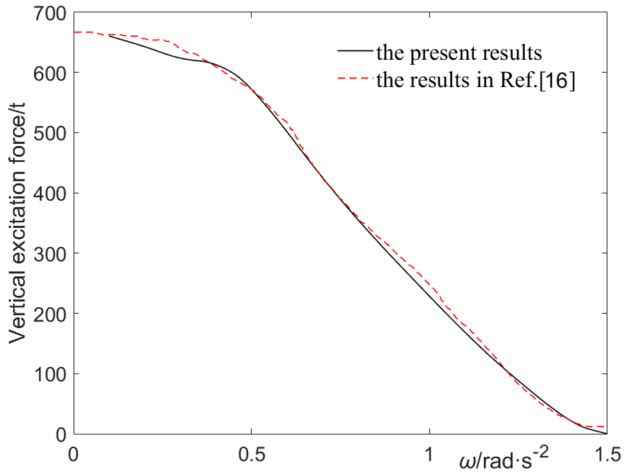

Fig. 4 Influence of wave frequency on the vertical force for the 4th pontoon (β=22.5°)

of incidence is equal to 0° and the wave period is 8 s. The black histograms show the result in Ref. [20], and the blue histograms represent the numerical solution obtained according to the computation procedure in the present study. Based on the present comparison, the reliability and the effectiveness of the presently applied procedure are illustrated.

3.2 The 67-type railway bridge

3.2.1 Response due to wave action

The following is a case study of the 67-type railway bridge crossing at the Jiyun Canal of the Jingshan Line during the emergency installation following the Tangshan earthquake in 1976. The bridge is 244.72 m long, of which the

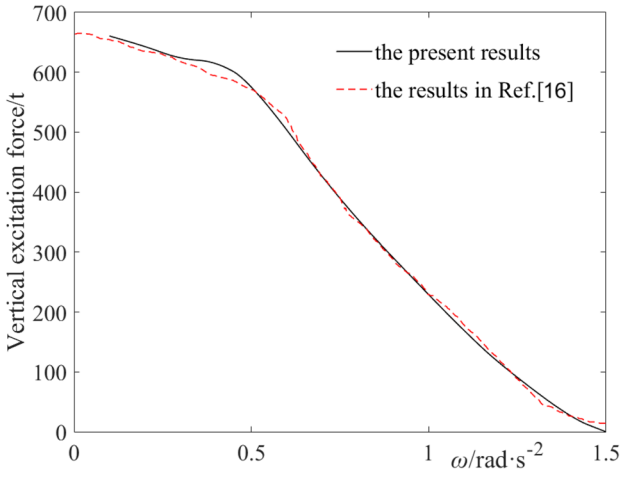

Fig. 5 Influence of wave frequency on the vertical force for the 4th pontoon (β=45°)

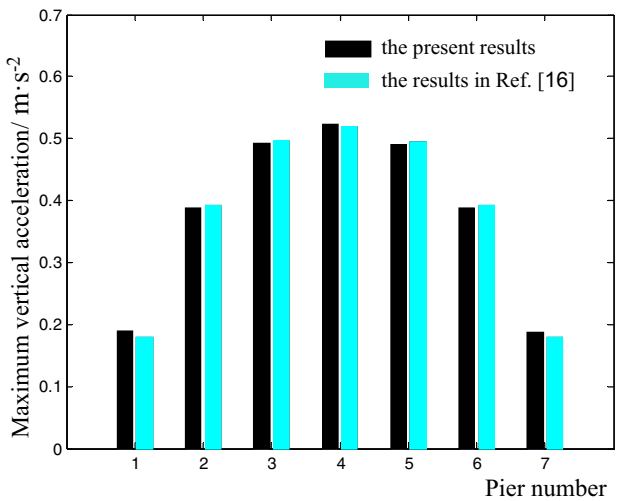

Fig. 6 Comparison results of the maximum vertical acceleration for each pontoon

Table 3 Main dimension of full-shaped pontoon

Length/m	Width/m	Draft/m	Weight/t
30.0	2.7	1.09	15.4

total length of the fixed trestle section is 25.7 m, the total length of the active trestle section is 101.56 m, the transition section is 68.56 m, and the span at the middle part of the river is 48.9 m. Assuming the floating bridge is under action of linear regular waves.

This section consists of ten groups of full-shaped pontoons, and the number within each group of full-shaped pontoons is shown in Fig. 1. The main dimension of each

Table 4 Main dimension of standard beam section

Length/m	Width/m	Height/m	A(area of section)/m^2	Weight/t
8.1	2.2	1.5	3.3	8.2
I_y(moment of inertia of section y-axis)/m^4	I_z(moment of inertia of section z-axis)/m^4	E(tensile modulus of elasticity)/GPa	G(shear modulus of elasticity)/GPa	μ(Poisson's ratio)
0.6981	0.4283	206	79.4	0.3

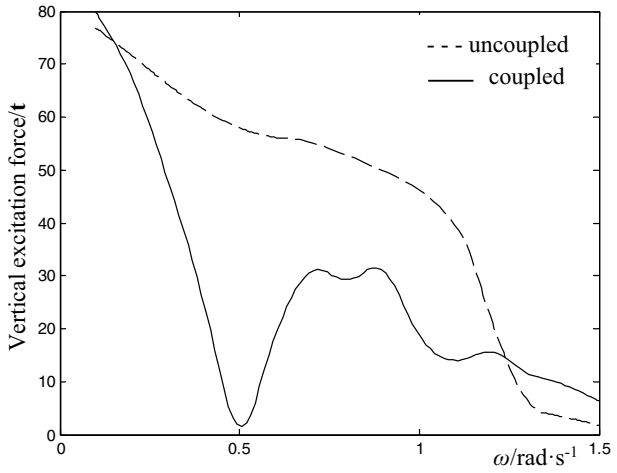

Fig. 7 Influence of wave frequency on the vertical force for the fifth pontoon (β=0°)

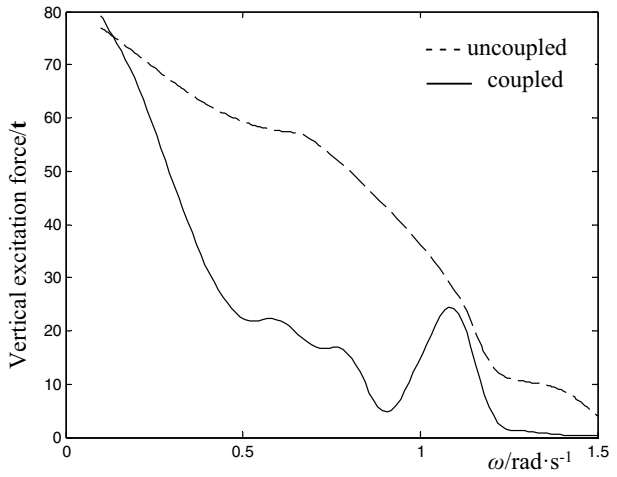

Fig. 8 Influence of wave frequency on the vertical force for the fifth pontoon (β=22.5°)

full-shaped pontoons and standard beam section are shown in Table 3 and 4. The average water depth at this section is 14 m and the wave height is 0.8 m, so it meets the linear wave theory.

The following calculations and analyses are performed using the fifth full-width pontoon near the mid-span as an example in order to study the influence of the hydrodynamic interaction between the other pontoons on this mid-span pontoon.

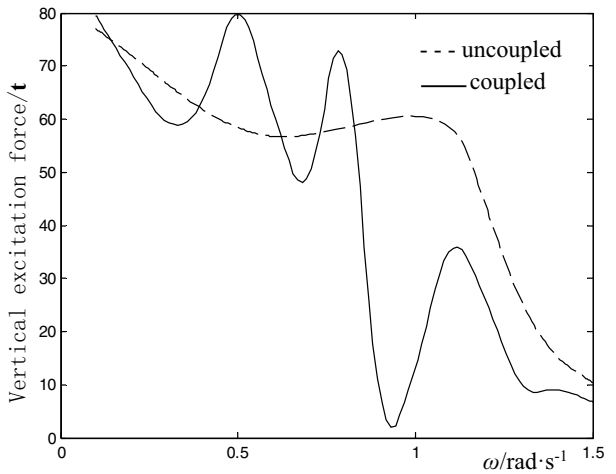

Fig. 9 Influence of wave frequency on the vertical force for the fifth pontoon (β=45°)

The single-factor analysis method is used to study the excitation force on the pontoon for different angles of wave incidence and different circular frequencies. Figures 7, 8, 9 show the changes in the force on the mid-span pontoon as a function of the circular frequency for waves at incidence angles of 0°, 22.5°, and 45°. The solid curve in the figure shows the vertical excitation force on the fifth pontoon considering the mutual interaction with the other pontoons; the dashed curve corresponds to the case that the interaction between the pontoons is not considered; only the vertical excitation force is calculated for the case without interaction.

As can be seen from Figs. 7, 8, 9, the two curves in each figure are very different, both in terms of general trends and specific values. This shows that the hydrodynamic interaction effects between the pontoons have a great impact on the excitation force, with very large fluctuations at certain circular frequencies. In turn, this will have an important effect on the motion of the structure. Due to the existence of radiation waves between the adjacent floating bodies, corresponding radiation forces will arise. Therefore, for a plurality of closely-spaced floating bodies in waves,

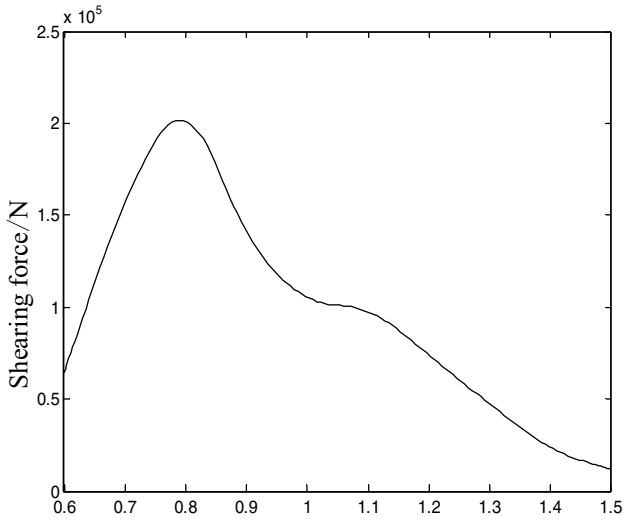

Fig. 10 Influence of wave frequency on the maximum shear force in the bridge girder

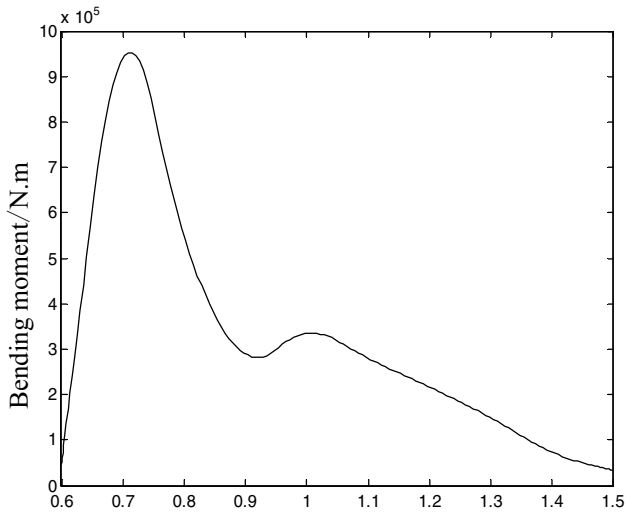

Fig. 11 Influence of wave frequency on the maximum bending moment in the bridge girde

the actual force levels are significantly different from those acting on a single body. From the analysis it is found that in addition to the influence of the wave incidence angle and from the circular frequency, this coupling effect is also closely related to the spacing between the pontoons [20]. Accordingly, at the design stage, the vertical excitation on the pontoon can be effectively reduced by reasonably adjusting the spacing between the pontoons.

Calculation of the internal forces in the bridge girder is an important part of the dynamic response analysis for the 67-type railway bridge. The actual stress condition in the girder can be calculated by determining the maximum shear force and bending moment values for different circular frequencies. Taking the 0° incident wave as an example, the maximum shear force and the maximum bending moment values for each section of the girder as a function of the wave circular frequency are calculated. The results are shown in Figs. 10 and 11. It can be seen from Fig. 10 that when the circular frequency of the wave is 0.8 rad/s, a maximum shear force of 2.01×10^5 N will be generated near the floating element of beam unit 2. The maximum shear stress will correspondingly occur at the middle section of the bridge girder (at the neutral axis). Similarly, as shown in Fig. 11, when the circular frequency of the wave is 0.74 rad/s, the maximum bending moment near the middle of the bridge span is 9.53×10^5 N·m. The maximum tensile stress is found at the bottom of the corresponding beam section (at the outer fiber of the cross-section).

Another important requirement in the design of the 67-type railway bridge is that the vertical acceleration of the bridge girder should not exceed 0.6 m/s^2. This limit is set to ensure safe passage of the traffic [1]. Calculating the vertical acceleration of the pontoons is also an important technical indicator in relation to design and analysis of this type of railway bridge. The following focuses on the changes in the vertical acceleration of the pontoons under the action of water waves with different circular frequencies and different angles of incidence. The graphs in a and b in Fig. 12 show the maximum vertical accelerations caused by incident waves at 0°, 30°, and 45° when the wave circle frequencies are 0.5 rad/s and 1 rad/s. It is obvious from the figure that when the angle of incidence is $\beta = 0$, the maximum vertical acceleration of each pontoon is larger than for the other cases. The reason for this phenomenon is that when $\alpha = 0$, the phase difference of the wave excitation forces on the pontoons is zero, which will cause the structure to respond with a high total vertical acceleration. For $\alpha \neq 0$, the motion displacement and acceleration of the pontoons will decrease due to the resulting phase difference. However, for this case, the torsional acceleration or torsional moment of the bridge may obtain their maximum values.

3.2.2 Response due to moving train loads

It is assumed that the 67-type railway pontoon bridge carries the standard live load of the Chinese Standard-18(show in Appendix I) without incident waves. Assuming that the train moves from the left to the right, and that the speed is 15 km/h, Fig. 13 below shows the variation of the vertical displacement of each pontoon as a

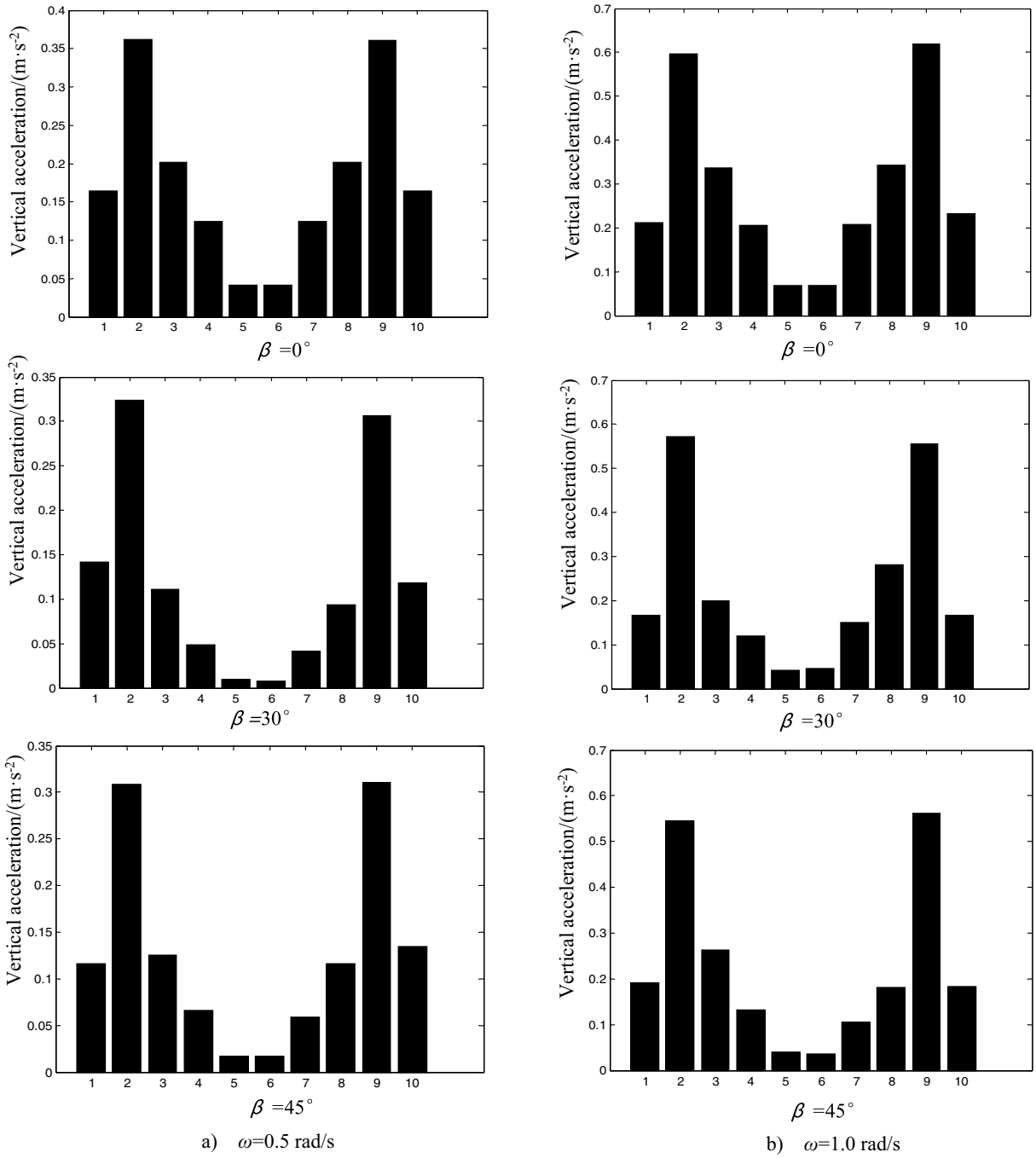

Fig. 12 Vertical acceleration of pontoons for different angles of incident wave

function of time. Taking pontoon number 1 as an example, Fig. 14 displays the vertical displacement of that pontoon when the train speed is 10 km/h, 15 km/h and 20 km/h, respectively.

By comparing and analyzing the vertical displacement of the pontoon at different speeds in the figure, it can be seen that the maximum vertical displacement of the pontoon will increase with speed. When the train is running at a low speed (v = 10 km/h in the figure), a certain amount of damping is present, while for a high speed (v = 20 km/h), an increased vibration of the pontoon occurs.

Figure 15 shows the maximum tensile stress in the bridge girder at different moments in time when the train moves from the left to the right at a speed of 15 km/h. It can be seen from the figure that the maximum tensile stress is 195 MPa, which is less than the material's tensile

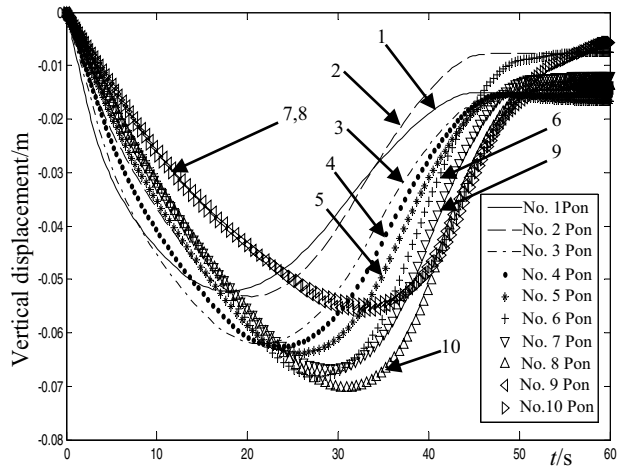

Fig. 13 Time history curve of vertical displacement for all pontoons (abbreviated as Pon.)

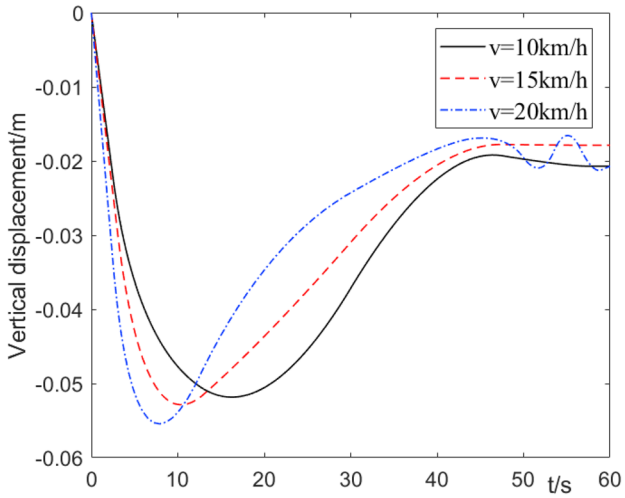

Fig. 14 Time history curve of vertical displacement for the first pontoon

strength design value of 230 MPa. Accordingly, the maximum occurring tensile stress of the bridge girder meets the requirements. Figure 16 shows the maximum deflection of the bridge girder at different time instants when the train is moving from the left to the right at a speed of 15 km/h. As can be seen from the figure, the maximum rotation angle is 0.033 (33 ‰). According to the relevant provisions of the Technical Regulations for Railway Bridge Emergency Repair [20], the maximum value of the slope of the pontoon bridge should be less than or equal to 40 ‰ during the train passage, and accordingly the bridge structure meets the requirements given in the regulations.

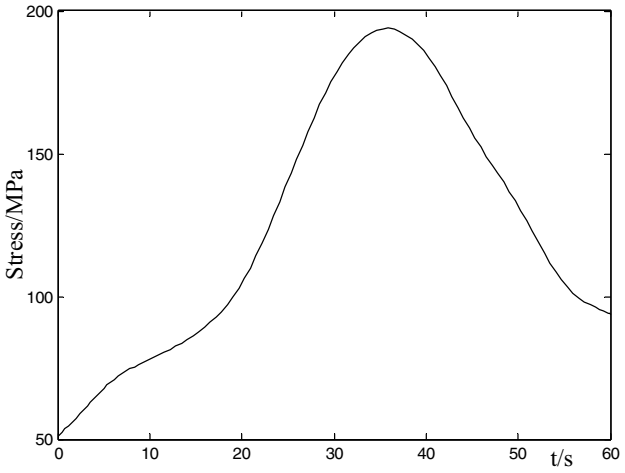

Fig. 15 Time history of maximum stress in the bridge girder

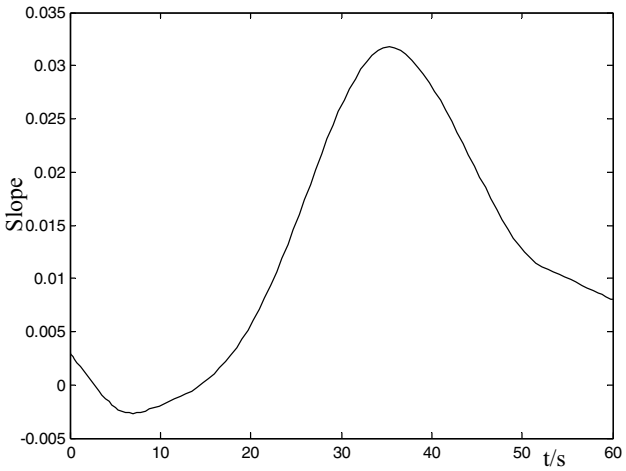

Fig. 16 Time history of the maximum rotation angle of the bridge girder

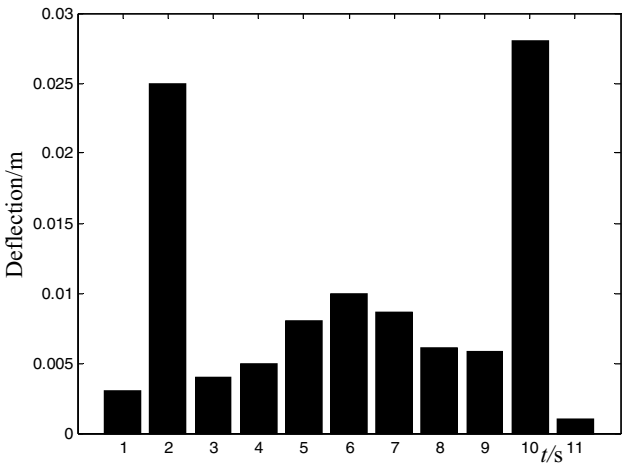

Fig. 17 Maximum deflection of each unit under moving train loads

Figure 17 shows the maximum deflection of the eleven beam segments in Fig. 1 during the crossing by the train. It can be seen that the maximum deflection of the bridge girder appears in the middle of unit 10, and it has a magnitude of 0.028 m.

4 Conclusion

Based on potential flow theory and the finite element method, this paper studies the dynamic characteristics of the 67-type railway floating bridge under the action of waves and train loads. According to the results of this paper, the method introduced is very different from the traditional 'beams on elastic foundation' theory. The wave parameters (such as the angle of incidence, circle frequency, etc.) will have a very strong impact on the displacement and internal load effects within the floating bridge. For example, for waves having the same angle of incidence, the magnitude of the vertical excitation force on the pontoon bridge will vary with the wave frequency. As a general trend, the magnitude of the excitation force will decrease as the circular frequency increases. Secondly, the hydrodynamic coupling effects between the pontoons will have a strong influence on the overall structural force. At certain frequencies, large fluctuations of the excitation forces will occur due to this interaction. This will have significant effects on the structural displacement, acceleration, and other response quantities. Thirdly, the speed of the train will have an important effect on the vertical displacement of the pontoons. When the train is moving at a low speed, there will be a certain amount of damping which is reduced for increasing speed levels. This also implies higher vibration amplitudes for increasing train speed. Both from the perspective of structural safety and in relation to driving comfort, such an increase of vibration amplitudes should be avoided as much as possible. It is believed that the present analysis approach has a more universal applicability than just for the study of one particular bridge type, such that it can provide theoretical and technical support for development of the next-generation floating pontoon railway bridges.

Acknowledgements The authors wish to express gratitude for support from the National Key R&D Program of China (Grant Number: 2021YFB2600605, 2021YFB2600600), and the Overseas Scholar Program in the Hebei Province (C20190514), from the State Key Laboratory of Mechanical Behavior and System Safety of Traffic Engineering Structures Project (ZZ2020-20), from the Youth Foundation of Hebei science and technology research project QN2018108.

Funding The authors have not disclosed any funding.

Declarations

Conflict of interests The authors declare that they have no known competing financial interests or personal relationships that could appear to influence the work reported in this paper.

Ethical Statement The authors declare that this article does not contain any studies with human participants or animals performed by any of the authors.

Appendix I

Brief introduction to the 67-type railway pontoon bridge

As the first generation of self-developed emergency repair equipment for pontoon bridge in China, the 67-type railway pontoon bridge is the main existing reserve pontoon bridge equipment in China, and it has played an important role in the rushing construction of many lines since the production stereotypes in 1967. The successful erection and opening of the 67-type railway pontoon bridge, especially in the rescue after Tangshan earthquake in 1976, ensured the restoration and operation of Beijing and Shandong railway line, the transportation of wounded and supplies, and also saved a great amount of time for the subsequent earthquake relief work. The smooth opening of this bridge was the first time that the 67-type railway pontoon bridge has been successfully applied in emergencies, and also used the standard pontoon bridge for railway train passing over in the 100-year history of China's railway. Based on the above-mentioned great success, the 67-type railway pontoon bridge won the first prize of scientific and technological achievements of railway corps at the National Science Conference in 1978.

As a kind of water engineering facilities and transportation ships in capital construction projects, the 67-type railway pontoon bridge had produced certain benefits to the national economy. Practice has proved that the 67-type railway pontoon bridge plays a significant part in the emergency repair and water engineering construction at ordinary times Figs. 18, 19.

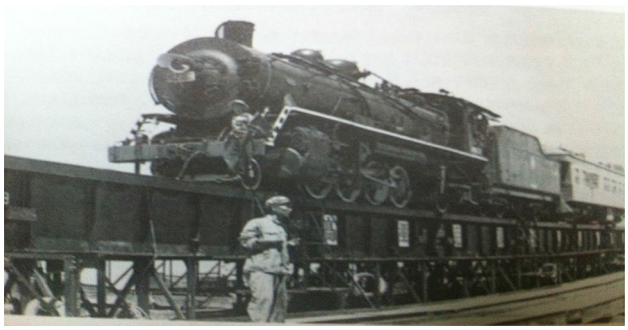

Fig. 18 Opening test of the 67-type railway pontoon bridge

Fig. 19 Opening traffic of the 67-type railway pontoon bridges

Relevant standards of moved train load for emergency bridge

It is customary to use ordinary live load and special live load to simulate the railway loads. Among them, ordinary live load is the weight of locomotive and vehicle; special live load refers to some concentrated axle load. According to the different types of trains, the axle load and wheelbase will not be the same. In the design, the live load standard of the train specified in the design specification should be strictly followed. This kind of live load should not only meet the actual situation of the current train load, but also consider the future development.

As early as 1920s, China firstly issued the relevant live load standards for trains. At that time, the American Cooper E-50 live load system was mainly referenced by train load, and was changed to metric system. In the front, two steam locomotives were coupled with coal-water vehicles. The axle load of the train was 22.5t, the wheelbase was 1.5 m, and the live load of the rear vehicle was 7.5t/m. Since then, *China Railway Bridge Locomotive Live Load* (hereinafter referred to as China's 20th class live load) published in 1938 reduced the axle load of the front train to 20t and the rear live load to 7t / m. After the founding of new China, with the rapid development of China's railway construction, the former Ministry of Railways formulated the live load standard of medium-Z level in railway load in 1951 (as shown in Fig. 20, in which Z represents the axle load of train, also known as live load level. In accordance with the different line grades and structure types, the axle load Z can be classified into three categories: 18t, 22t and 26t,while the effect of the other locomotive and two coal water tankers is replaced by a uniform load of 30 m long and distributed concentration of 0.42Zt/m, and the distribution concentration of vehicle live load is 0.3Zt/m. The live load standard provides an effective basis for the railway design in the early days of the people's Republic of China. The railway load of the floating bridge at the initial stage of design is set as medium-18 live load standard [20].

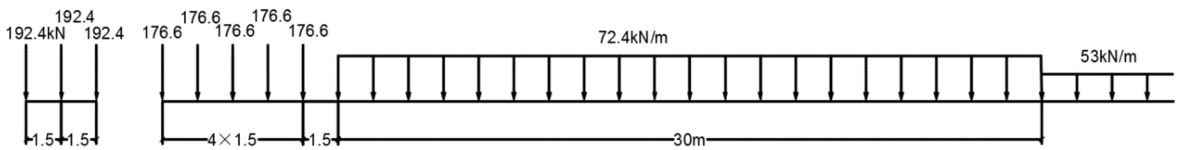

Fig. 20 the live load of the Chinese Standard-18 (unit:m)

References

1. Zhang Z, Xin S (2001) Railway floating bridge[M]. China Railway Publishing House, Beijing (**in Chinese**)
2. Wang J (2012) Design theory of pontoon[M]. National Defence Industry Press, Beijing (**in Chinese**)
3. Xin S (1995) Overall Analysis of the railway bridge structure. Railway Construction Technol 6:51–54 (**in Chinese**)
4. Zhang J., Miao G (2007) Hydroelastic behavior of a ribbon pontoon bridge with different water depths[J]. Journal of Hydrodynamics (Ser.A), 6:118–123 (**in Chinese**)
5. Mukherji B (1995) Dynamic behavior of a continuous floating bridge[D]. University of Washington, Washington
6. Shi L, Lin Z, Cui W (2003) Vibration response of a moored multi-span uniform floating bridge under a moving load. Ocean Eng 7:65–67 (**in Chinese**)
7. Wang X. Research on numerical simulation of mechanical characteristics for 67-type railway pontoon bridge[D].Shijiazhuang: Shijiazhuang Tiedao university. (**in Chinese**)
8. Hartz BJ. and Mukherji B (1971) Response of Floating Bridges to Random Wave Forces. In ASCE-ASME National Transportation Engineering Conference, Seattle
9. Langen I, Sigbjörnsson R (1980) On stochastic dynamics of floating bridges. Engineering Structures 2(4):209–216. https://doi.org/10.1016/0141-0296(80)90002-4
10. Watanabe E (2003) Floating bridges: past and present types of floating bridge. Struct Eng Int 2:128–132
11. Li Q, Wang J (2006) Analysis of the dynamical response of floating bridges under wave influence. Eng Equipment Res 6:39–43 (**in Chinese**)
12. Giske FI G, Kvåle KA, Leira BJ, Øiseth O (2018) Long-term extreme response analysis of a long-span pontoon bridge. Marine Structures 58:154–171. https://doi.org/10.1016/j.marstruc.2017.11.010
13. Xiang X, Viuff T, Leira B, Øiseth O (2018) Impact of hydrodynamic interaction between pontoons on global responses of a long floating bridge under wind waves. In: Proceedings of the 37th international conference on ocean, offshore and arctic engineering, pp 1–11. https://doi.org/10.1115/OMAE2018-78625.
14. Lin Z (2006) Analysis of pontoon-vehicle vibration response based on ABAQUS software. Eng Equipment Res 8:105–109 (**in Chinese**)
15. Wang B, Chen X, Jiang Z, Huang Y, Gao F (2013) Dynamic responses of Ribbon Bridge subjected to different moving loads. Chinese J Appl Mech 1:29–33 (**in Chinese**)
16. Seif M, Inoue Y (1998) Dynamic analysis of floating bridges. Marine Structures 11(1–2):29–46. https://doi.org/10.1016/S0951-8339(97)00012-9
17. Cheng Z, Gao Z, Moan T (2018) Hydrodynamic load modeling and analysis of a floating bridge in homogeneous wave conditions[J]. Mar Struct 59:122–141
18. Sha Y, Amdahl J, Aalberg A et al (2018) Numerical investigations of the dynamic response of a floating bridge under environmental loadings[J]. Ships and Offshore Structures 13(sup1):113–126
19. Dai J, Stefanakos C, Leira BJ et al (2021) Effect of modelling inhomogeneous wave conditions on structural responses of a very long floating bridge[J]. J Marine Sci Eng 9(5):548
20. China Railway Third Survey and Design Institute Group Co. Ltd. Technical Regulations for Emergency Repair (construction) of Railway Bridges, 2003. (**in Chinese**)
21. Deji L (2011) The record of the development of the 67-type railway boat bridge. Traffic Engineering and Technology for National Defence 4:69–72 (**in Chinese**)